

Molecule Cascades

A. J. Heinrich,*† C. P. Lutz,* J. A. Gupta, D. M. Eigler

Carbon monoxide molecules were arranged in atomically precise configurations, which we call "molecule cascades," where the motion of one molecule causes the subsequent motion of another, and so on in a cascade of motion similar to a row of toppling dominoes. Isotopically pure cascades were assembled on a copper (111) surface with a low-temperature scanning tunneling microscope. The hopping rate of carbon monoxide molecules in cascades was found to be independent of temperature below 6 kelvin and to exhibit a pronounced isotope effect, hallmarks of a quantum tunneling process. At higher temperatures, we observed a thermally activated hopping rate with an anomalously low Arrhenius prefactor that we interpret as tunneling from excited vibrational states. We present a cascade-based computation scheme that has all of the devices and interconnects required for the one-time computation of an arbitrary logic function. Logic gates and other devices were implemented by engineered arrangements of molecules at the intersections of cascades. We demonstrate a three-input sorter that uses several AND gates and OR gates, as well as the crossover and fan-out units needed to connect them.

The scanning tunneling microscope (STM) can be used to build atomically precise structures and investigate their physical and functional properties. Here we present a class of nanometer-scale structures, "molecule cascades," that are both instructive (they enable detailed studies of adsorbate motion) and functional (they perform computation).

The motion of single atoms and molecules on surfaces can be studied in a well-characterized environment with the STM (1). We investigated the hopping mechanism of CO molecules in molecule cascades through studies of the hopping rate as a function of temperature, isotope, and local environment. We found that at temperatures below 6 K, the hopping motion of CO molecules in our cascades was due to quantum tunneling of the molecule between neighboring binding sites on the surface. The importance of quantum tunneling in hydrogen diffusion (2) was recently demonstrated in an STM study of hydrogen atoms on a Cu(100) surface (3, 4). In contrast to the random walk of diffusion, the tunneling rate can be engineered in molecule cascades by controlling the hopping direction and interactions with neighboring molecules. At higher temperatures, we observed thermally activated hopping with an anomalously low Arrhenius prefactor, which we interpret as being due to tunneling of the CO molecule from a vibrationally excited state.

Although the silicon transistor technology on which modern computation is based has shown rapid exponential improvement in speed and integration for more than four de-

acades, it is widely expected that this improvement will slow as devices approach nanometer dimensions (5). The search for functional nanometer-scale structures has led to the exploration of many alternative computation schemes, most of which, like the silicon transistor, are based on gating the flow of electrons. Such novel systems include quantum dots (6), organic molecules (7), carbon nanotubes (8), nanowires (9), and the motion of single atoms or molecules (10). However, alternative computation schemes that operate on different principles have also been proposed, among them electrons confined in quantum dot cellular automata (11, 12), magnetic dot cellular automata (13), and solutions of interacting DNA molecules (14). Computation can also be achieved with purely mechanical means (15), as exemplified by the calculating engines of Babbage (16). The toppling of a row of standing dominoes can also be used to perform mechanical computation. Tipping a single domino causes many others to topple sequentially. Such a domino cascade can be used for the one-time transport of a single bit of information from one location to another, with the toppled and untoppled states representing binary 0 and 1, respectively. Dominoes can be set in patterns that perform logic operations. Here we demonstrate an analogous form of mechanical computation on the nanometer length scale with molecule cascades in which we implemented all of the logic gates and interconnections required to perform the one-time calculation of an arbitrary logic function.

Apparatus and methods. The data presented here were acquired with low-temperature ultrahigh-vacuum STMs: one fixed at 5 K, and one that is variable in temperature between 0.5 and 40 K. The variable-temperature STM uses a novel continuous-circula-

tion ^3He refrigerator for temperatures from 1.0 to 4.5 K. Below 1.0 K, the STM operates in a single-shot mode with a hold time of 10 hours. Helium-3 is liquefied without the need for a pumped ^4He bath (a so-called "1 K pot") through the use of the Joule-Thompson effect and counterflow heat exchange. Operation up to ~ 40 K is easily achieved with a small heater on the microscope stage. Clean Cu(111) single-crystal surfaces were prepared by repeated Ar sputtering and heating in ultrahigh vacuum to 600°C , after which the Cu crystal was transferred to the cold STM. CO molecules were adsorbed onto the Cu surface by admitting CO gas with the crystal held at 15 K (17). We found that CO molecules did not appear in our STM images when adsorbed on a surface below ~ 10 K. We coadsorbed $^{12}\text{C}^{16}\text{O}$ and $^{13}\text{C}^{16}\text{O}$ by mixing isotope-selected gases in the room-temperature vacuum chamber (18). The STM tips were polycrystalline Ir. STM images were typically recorded at a sample bias voltage of $V = 10$ mV and a tunnel current of $I = 1$ nA. We manipulated CO by decreasing the tunnel-junction resistance to ~ 250 kilohms,

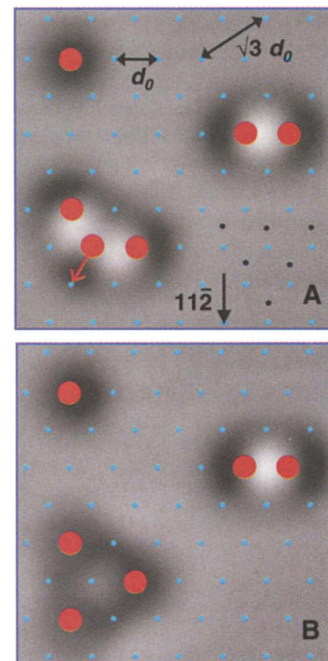


Fig. 1. STM images (1.9 nm by 1.9 nm) of CO molecules on a Cu(111) surface ($I = 1$ nA; $V = 10$ mV). The gray-scale images represent the curvature of the tip height, so local peaks appear light and local dips appear dark. Solid red circles indicate locations of CO molecules. Blue dots indicate surface-layer Cu atoms, and black dots indicate second-layer Cu atoms. d_0 is the Cu-Cu distance, 0.255 nm. (A) An isolated CO molecule (top left), a dimer (right), and a trimer in the chevron configuration (bottom left). The arrow indicates how the central CO molecule in the chevron will hop spontaneously, typically within a few minutes at 5 K. (B) The same area after the CO molecule has hopped.

IBM Research Division, Almaden Research Center, 650 Harry Road, San Jose, CA 95120, USA.

*These authors contributed equally to this work.

†To whom correspondence should be addressed. E-mail: heinrich@almaden.ibm.com

which brought the tip sufficiently close to a molecule to pull it across the surface (19).

The stability of CO on Cu(111). The CO molecule is useful for the construction of quantum corrals (20) on the Cu(111) surface because it is readily manipulated with the STM, stable at 5 K over a broad range of tunneling voltages, and only weakly binds to other CO molecules adsorbed to the surface. We were thus motivated to understand the stability of CO overlayer structures on the Cu(111) surface.

Some simple arrangements of CO molecules on the Cu(111) surface at 5 K are shown in Fig. 1. Although we did not resolve the surface Cu atoms under these imaging conditions, the Cu lattice (blue dots in Fig. 1) was inferred from the positions of CO because it is known that CO binds atop the surface Cu atoms, standing upright with the C atom closest to the Cu surface (17, 21). Consistent with the CO adsorption geometry, a CO monomer (Fig. 1, top left) images as an azimuthally symmetric dip, typically 0.05 nm deep (22). An isolated CO monomer is completely stable at 5 K; the onset of thermal diffusion on the Cu(111) surface is ~ 40 K (17). Two CO molecules positioned at nearest neighbor sites (Fig. 1, right) appear as dips centered at Cu lattice sites with a bright area directly between them. We refer to this arrangement as a “dimer.” The CO dimer was also stable at 5 K, although the molecules could be easily separated with the STM tip (1,

23). There are three possible configurations of a CO trimer on the Cu(111) surface: a three-fold symmetric, close-packed arrangement in which the molecules are all nearest neighbors to each other; a bent-line configuration as illustrated in Fig. 1A (bottom left); and a straight-line configuration. We found that these trimers exhibit a hierarchy of stability. The close-packed structure is entirely stable at 5 K. The bent-line configuration shown in Fig. 1 is stable enough to image but decays spontaneously in a few minutes by the indicated hop of the central molecule. The straight-line configuration decays on a time scale on the order of 1 s. We will make extensive use of the bent-line arrangement of three molecules and refer to it as a “chevron.” Chevrons decay only as shown, but the rate depends sensitively on the arrangements of nearby CO molecules. After a chevron has decayed, the molecules are all $\sqrt{3}$ lattice sites apart. This appears to be a low-energy spacing, on the basis of the $\sqrt{3}$ by $\sqrt{3}R30^\circ$ island formation observed at higher temperatures (17).

Molecule cascades. We produced a cascade of hops by arranging CO molecules in staggered chains of dimers (Fig. 2). The cascade was initiated by moving a “trigger” CO molecule with the STM tip to form an initial chevron. This newly formed chevron then spontaneously decays and forms yet another chevron, and so on for a cascade of any length. This “linked-chevron” cascade prop-

agates forward reliably because the energy of the system is lowered each time a molecule hops to a new site on the surface. If the energy of the system were not lowered with each hop, then we would have observed hops that are backward (toward the initial state) as often as forward. We observed only forward hops in linked-chevron cascades, but saw occasional backward hopping in the cross-over structure (described below). In general, there is no lower limit to the average energy that must be dissipated with each hop: As this energy drops below the thermal energy, backward hops become common, and the propagation time increases.

The linked-chevron cascade shown in Fig. 2A also contains CO molecules that speed up the cascade. These molecules are not part of a dimer in the initial configuration and do not become part of a chevron as the cascade propagates. We found that locating CO at the $\sqrt{3}$ distance from the site to which a hopping CO molecule moves increases the hopping rate ~ 100 -fold, consistent with the observation that the $\sqrt{3}$ spacing is apparently a low-energy configuration.

The hopping mechanism. Understanding the hopping mechanism underlying the decay of the chevron is not only of fundamental value; it can also be of practical value in the rational design of cascade structures. Toward this end, we measured the temperature dependence of the hopping rate. To facilitate the comparison of our results with theoretical calculations, we would ideally measure the hopping rate of an isolated chev-

Fig. 2. Linked-chevron cascade. (A) STM image (1.7 nm by 3.4 nm) of the initial arrangement of CO molecules. To start the cascade, we manually moved one CO molecule with the STM tip to set up a chevron, which decays after a certain time by the indicated hop (marked 0). The cascade spontaneously proceeds one hop at a time until all chevrons have decayed. (B) STM image after all chevrons have decayed. The CO molecules are now evenly spaced $\sqrt{3}d_0$ apart. (C) Example of a single timing measurement showing changes in tip height as a function of time t . We formed the initial chevron by bringing the tip closer to the surface (at $t = -1.5$ s) and moving a CO molecule to the right. The decay of this chevron is marked by a sharp drop in tip height (hop 0 in the inset) and defines $t = 0$. The tip was then retracted and quickly translated to the final position marked “F,” chosen so that the decay of the fourth chevron (hop 4 at $t = 11.6$ s) could be observed as a step up in tip height.

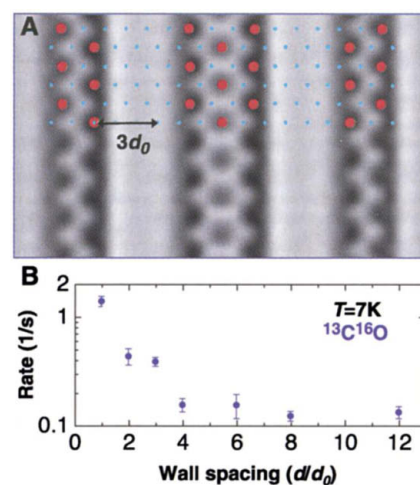
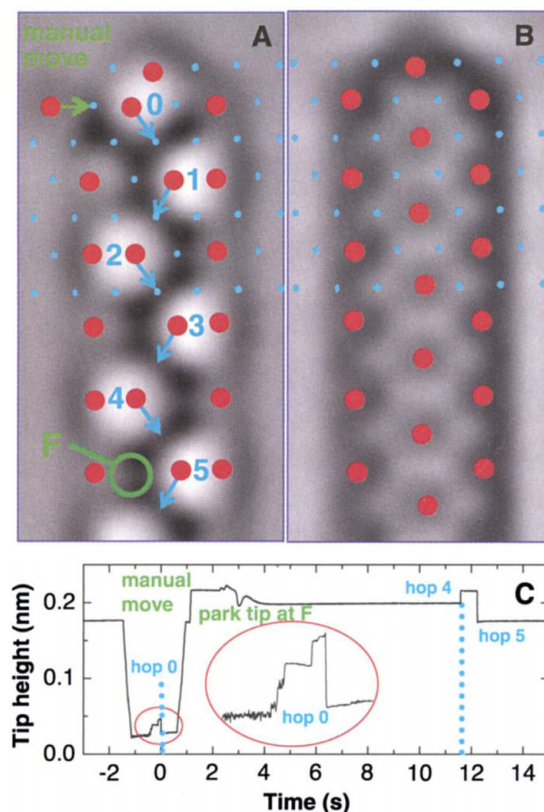


Fig. 3. Environmental influence on hopping rates. (A) STM image (5 nm by 3 nm) of the CO timing structure (center) with walls made of CO molecules on both sides. The wall spacing is $d = 3d_0$, where d_0 is the nearest neighbor spacing of the substrate atoms. A spacing of $d = 0$ corresponds to a continuous $\sqrt{3}$ by $\sqrt{3}$ array. (B) The hopping rate of $^{13}\text{C}^{16}\text{O}$ as a function of d . Error bars are based on the measured spread in five runs of a cascade with a length of 16 hops.

ron on a defect-free Cu(111) surface. However, we found that the presence of the STM tip influences the decay rate of chevrons under all accessible tunneling conditions. Thus, the decay rate of an isolated chevron cannot be reliably measured by repeated imaging or holding the tip fixed in proximity to the chevron and detecting a change in tunneling resistance when the molecule hops (24).

To minimize tip proximity effects, we constructed linked-chevron cascades as shown in Fig. 2 and used the STM only to start the cascade by moving the trigger molecule and to detect a characteristic signal near the end of the cascade when the last CO hops (Fig. 2C). The hopping rate is equal to the number of hops in the cascade divided by the average measured propagation time. The choice of tip trajectory during each timing measurement ensured that the molecules under test, with the exception of the last hop, were at least 0.7 nm laterally away from the tip at all times. Tip influences can be further reduced by increasing the length of the cascade.

We found the measured hopping rate in linked-chevron structures to be sensitive to the influence of the local environment, such as nearby defects, steps, impurities, surface-state standing waves (25), and other CO molecules not part of the linked-chevron structure. This observation is consistent with our

conclusion (see below) that the hopping is due to quantum tunneling of the molecule, with tunneling rates being exponentially sensitive to the height and width of the energy barrier. To eliminate variations in the hopping rate due to environmental influences, we enclosed the cascade with walls of CO molecules (Fig. 3A). As shown in Fig. 3B, the hopping rate is independent of wall spacing d for $d > 4d_0$, where d_0 is the Cu nearest neighbor distance, but increases by a factor of 10 as d is reduced to d_0 .

The crystal orientation (indicated in Fig. 1) also substantially affects CO hopping rates. Linked-chevron cascades made to propagate in the $(\bar{1}\bar{1}2)$ direction proceed at a rate (at 6 K) that is one-eighth the rate of cascades made to propagate in the $(11\bar{2})$ direction, as shown in Figs. 2 and 3, indicating that the orientation of second-layer Cu atoms is important.

Another source of systematic error that could affect our hopping rate measurements comes from the variation in mass of the CO molecule due to the $\sim 1\%$ natural isotopic abundance of ^{13}C . To eliminate this error from measurements and to test for the mass dependence of the hopping rate, we used inelastic electron tunneling spectroscopy (IETS) (26–28) of CO vibrational excitations (29, 30) to build structures in which the C isotope of each molecule was individually

selected (Fig. 4). We observed a shift with C isotope (^{12}C versus ^{13}C) of 1.0 meV for the CO frustrated rotation mode at ~ 35 meV and no isotope shift for the frustrated translation mode at 4 meV (31). The isotope selection works by assembling an array of CO molecules (Fig. 4C), imaging the array with IETS (Fig. 4D), and using the isotope dependence of the frustrated rotation mode to determine the C isotope of each CO molecule. This information was then used to build isotope-selected structures. IETS peaks were initially correlated to C isotopes by dosing $^{12}\text{C}^{16}\text{O}$ and $^{13}\text{C}^{16}\text{O}$ separately on clean surfaces. We could not confidently distinguish O isotopes with IETS and rely on a low initial concentration of the undesired isotopes ^{17}O and ^{18}O . To further rule out substantial contributions from O isotopes, we routinely performed consistency checks between hop rates of different groups of CO.

A comparison of hopping rates for $^{12}\text{C}^{16}\text{O}$ and $^{13}\text{C}^{16}\text{O}$ linked-chevron cascades is shown in Fig. 5. All timing measurements were performed in the same location by swapping the CO isotopes in and out. The hopping rate for each isotope is independent

Fig. 4. Sorting CO isotopes. (A) Inelastic electron tunneling spectroscopy (d^2I/dV^2) of CO molecules in a $\sqrt{3}$ by $\sqrt{3}$ array. The blue and red curves were taken on top of a $^{13}\text{C}^{16}\text{O}$ molecule and a $^{12}\text{C}^{16}\text{O}$ molecule, respectively. Each curve shows two peaks at positive voltage and two inverted peaks at negative voltage. These peaks are due to vibrational excitations corresponding to the frustrated translation mode ($|V| = 4$ mV) and the frustrated rotation mode ($|V| = 35$ mV). (B) The frustrated translation mode at positive voltage in the dI/dV spectrum. (C) STM topograph (4.6 nm by 5.7 nm) of a $\sqrt{3}$ by $\sqrt{3}$ array of CO. (D) dI/dV image acquired simultaneously with the topograph at $V = 35.5$ mV, $I = 3.55$ nA, and $V_{AC} = 1.5$ mV_{RMS}. Bright and dark peaks correspond to $^{13}\text{C}^{16}\text{O}$ and $^{12}\text{C}^{16}\text{O}$ molecules, respectively. a.u., arbitrary units.

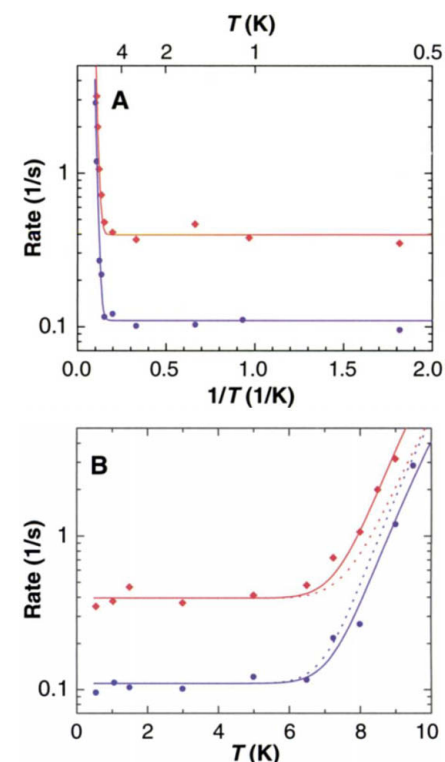
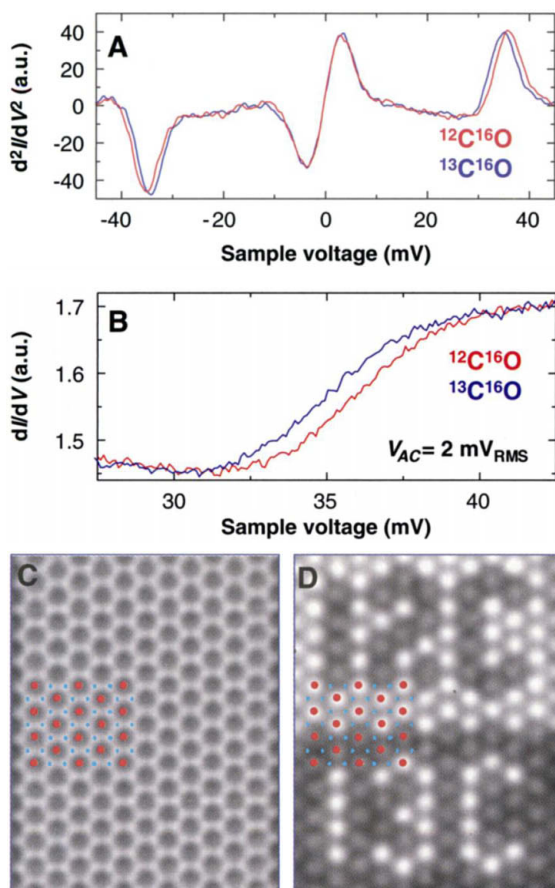


Fig. 5. Comparison of $^{12}\text{C}^{16}\text{O}$ and $^{13}\text{C}^{16}\text{O}$ hopping rates in a $(11\bar{2})$ oriented linked-chevron molecule cascade. The cascade was fully enclosed by CO walls located with a spacing of $d = 5.5d_0$ on the left and $d = 6d_0$ on the right (compare with Fig. 3). Each point represents the average for eight measurements of an 18-hop cascade. (A) Arrhenius plot of the hopping rate. (B) Same data, but on a linear temperature scale. Solid and dotted curves are least squares fits to Eq. 1.

of temperature below ~ 6 K. A pronounced isotope effect is evident in the low-temperature hopping rate R_{QT} of $0.396 \pm 0.018 \text{ s}^{-1}$ for $^{12}\text{C}^{16}\text{O}$ and $0.110 \pm 0.008 \text{ s}^{-1}$ for $^{13}\text{C}^{16}\text{O}$, a ratio of 3.6. Both findings are characteristic of quantum tunneling. A mixed-isotope cascade in which the molecules that hop are $^{12}\text{C}^{16}\text{O}$ and the rest are $^{13}\text{C}^{16}\text{O}$ gives a tunneling rate $R_{\text{QT}} = 0.41 \pm 0.03 \text{ s}^{-1}$, identical to that for a cascade in which all molecules are $^{12}\text{C}^{16}\text{O}$. This indicates that motion of the C atoms on neighboring molecules does not substantially influence the tunneling process. A simple analysis with the Wentzel-Kramer-Brillouin (WKB) approximation, assuming no isotope shift of the zero-point energy (ZPE), yielded a tunneling mass ratio of 1.087. This led to the unexpected result that the tunneling mass is 13 atomic mass units (amu) for $^{13}\text{C}^{16}\text{O}$ and 12 amu for $^{12}\text{C}^{16}\text{O}$ (assuming a tunneling mass difference of 1 amu). Hence, if the isotope ZPE shift is small enough to be ignored, the relevant tunneling mass is that of the C atom rather than the entire CO molecule (32). Further study is needed to determine whether the isotope ZPE shift is small enough to be ignored.

The temperature dependence of the hopping rate above 6 K approaches a linear slope

in an Arrhenius plot (Fig. 5A), which indicates a thermally activated process. We model the hopping rate R of each CO isotope as the sum of the tunneling rate R_{QT} and a thermally activated rate

$$R = R_{\text{QT}} + A \exp(-E/k_{\text{B}}T) \quad (1)$$

where A is the Arrhenius prefactor, E is the activation energy, and k_{B} is the Boltzmann constant. Fitting the hopping rates for both isotopes with the same values for A and E yields a poor fit (dotted lines in Fig. 5B) because of the strong isotope dependence that persists to the highest temperatures measured. This implies that the thermally activated process is dependent on the C isotope.

The isotope dependence can be attributed to the prefactor and/or activation energy. Allowing a separate prefactor (A) for each isotope produces an excellent fit (Fig. 5, A and B, solid lines) and yields $E = 9.5 \pm 0.9 \text{ meV}$ for both, with $A = 10^{5.8 \pm 0.5} \text{ s}^{-1}$ for $^{12}\text{C}^{16}\text{O}$ and $A = 10^{5.4 \pm 0.5} \text{ s}^{-1}$ for $^{13}\text{C}^{16}\text{O}$. Instead permitting separate activation energies (E) produces a nearly indistinguishable fit. Therefore, these measurements cannot directly determine the relative importance of these two parameters.

If the thermally activated behavior observed is due to classical (over-the-barrier)

hopping, then the activation energy represents the barrier height relative to the molecule's energy in the initial potential well. In this case, the isotope dependence in E can arise from an isotope shift in ZPE of the molecule in its initial potential well: The lighter molecule will have a higher initial energy and a correspondingly lower energy barrier (33, 34). The entire set of hopping rates in Fig. 5 can be modeled with an isotope shift in the ZPE of 0.7 meV ($E = 8.9 \pm 0.9 \text{ meV}$ for $^{12}\text{C}^{16}\text{O}$ and $E = 9.6 \pm 0.9 \text{ meV}$ for $^{13}\text{C}^{16}\text{O}$) and a shared prefactor of $10^{5.5 \pm 0.5} \text{ s}^{-1}$. However, we do not think that over-the-barrier hopping provides an adequate description because the observed prefactor is anomalously low. The prefactor for an over-the-barrier hopping process is the attempt rate, which should be comparable to initial-state vibrational frequencies (35). We expect vibrational frequencies for CO in the chevron potential well to be comparable to the frequencies for isolated CO on Cu, which are 10^{12} to 10^{13} s^{-1} . Observed prefactors for classical thermal diffusion nearly always fall in the range from 10^{10} to 10^{15} s^{-1} (36, 37). Quantum tunneling can show temperature dependence (and a low prefactor) when lattice vibrations are needed to compensate for static lattice relaxation induced by the adsorbate in

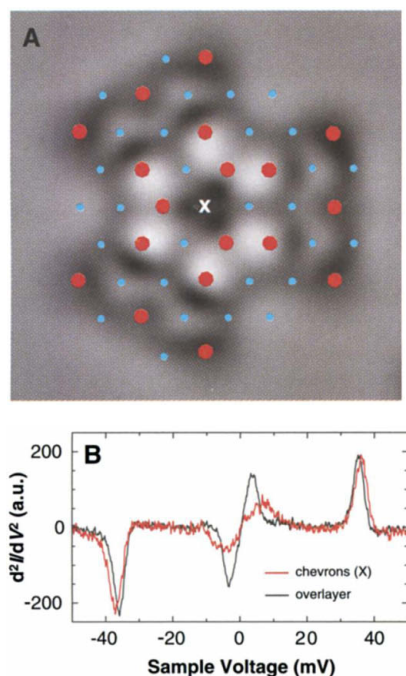


Fig. 6. Modified CO vibrational excitation spectrum in a stabilized-chevron structure. (A) STM image (2.3 nm by 2.3 nm) of $^{12}\text{C}^{16}\text{O}$ assembled in the chevron structure. $V_{\text{DC}} = 10 \text{ mV}$; $I_{\text{DC}} = 1.0 \text{ nA}$; $T = 5 \text{ K}$. (B) d^2I/dV^2 spectrum with the tip at position "X" in (A), compared with the spectrum of a $\sqrt{3}$ by $\sqrt{3}$ overlayer. $V_{\text{AC}} = 0.5 \text{ mV}_{\text{RMS}}$. For clarity, the frustrated rotation mode ($|V| = 35 \text{ mV}$) of the chevron spectrum was normalized to that of the overlayer.

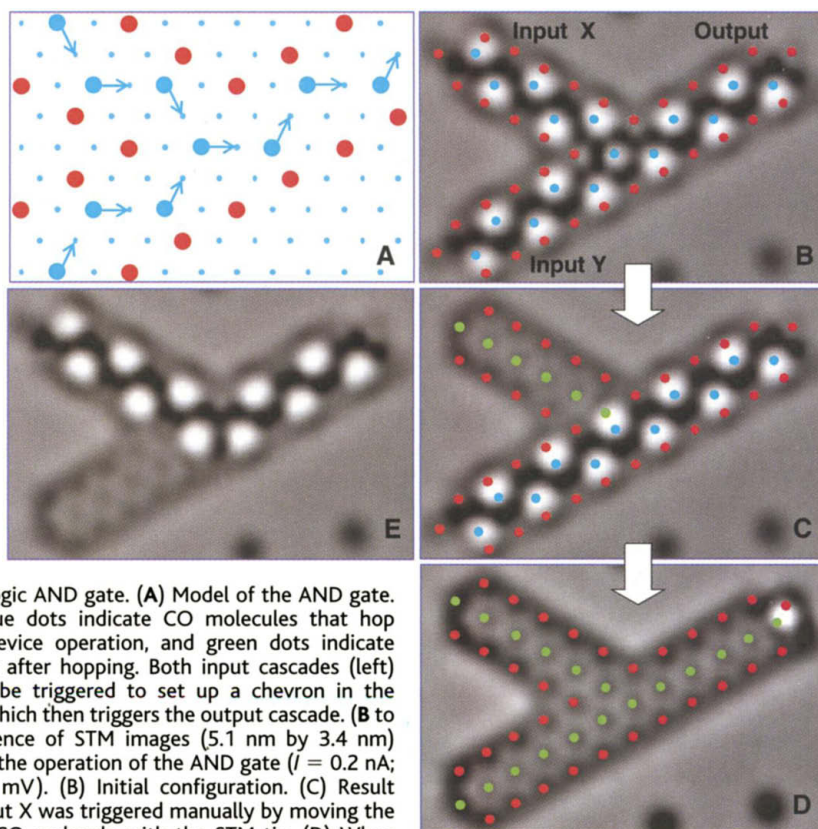


Fig. 7. Logic AND gate. (A) Model of the AND gate. Large blue dots indicate CO molecules that hop during device operation, and green dots indicate positions after hopping. Both input cascades (left) have to be triggered to set up a chevron in the center, which then triggers the output cascade. (B to D) Sequence of STM images (5.1 nm by 3.4 nm) showing the operation of the AND gate ($I = 0.2 \text{ nA}$; $V = 10 \text{ mV}$). (B) Initial configuration. (C) Result after input X was triggered manually by moving the top left CO molecule with the STM tip. (D) When input Y was triggered, the cascade propagated all the way to the output. (E) The result of manually resetting all CO molecules to the initial configuration of (B), and then manually triggering input Y. Subsequently triggering input X yielded configuration (D).

its initial potential well (3, 38), but this type of thermally assisted tunneling cannot be responsible for our observations because we directly observed temperature-independent tunneling. Low prefactors that have not been attributed to tunneling include $4 \times 10^7 \text{ s}^{-1}$ for the diffusion of CO on Cu(110) (1) and values as low as $2 \times 10^3 \text{ s}^{-1}$ for STM measurements of metal atom diffusion (36), but the latter results are disputed (35).

We suggest that the low prefactor we report is the result of tunneling from thermally excited states of the molecule. The prefactor in such a model is the product of the tunneling attempt rate (39) and the probability of tunneling through the remaining barrier when starting from the excited state. This tunneling probability, and hence the prefactor, should show a strong mass dependence. Applying this model of thermally assisted tunneling to our cascades means that the activation energy of 9.5 meV must correspond to the energy of an excited vibrational state of the molecule that hops. We cannot perform IETS directly on chevrons because the hop-

ping rate is too fast. However, vibrational measurements can be made in related “stabilized-chevron” structures, such as that in Fig. 6. Here the hopping of any chevron is hindered by the influences of the two neighbor chevrons. IETS with the STM tip at the center of the structure primarily comprises the average vibrational spectrum of the three identical CO molecules near the center. There is a substantial upward shift (and a broadening or splitting) of the frustrated translation mode at $|V| < 10 \text{ mV}$, when compared to a $\sqrt{3}$ overlayer (Fig. 6B). This suggests that a modified frustrated translation vibrational energy of 9.5 meV for chevrons in molecule cascades is reasonable.

At higher temperatures, the thermally assisted tunneling model predicts a further increase of slope in the Arrhenius plot when direct over-the-barrier processes or higher vibrational states become thermally excited. Tunneling from thermally excited states has previously been observed for H atoms in doped solid Xe, which shows a prefactor of only $\sim 10^4$ and an activation energy that

matches the H atom vibrational frequency (40). The data presented here may be the result of isotope ZPE shift and thermally assisted tunneling acting together.

Cascade logic circuits. A molecule cascade serves as a wire to communicate one bit of information across the surface: A molecule in its initial or final position represents binary 0 or 1, respectively. The cascades can also serve as logic gates. The operation of a logic AND gate whose inputs and outputs are linked-chevron cascades is shown in Fig. 7. The core element of the AND gate is simply a chevron trimer. The central CO molecule becomes part of a chevron only if cascades have propagated along both input arms. Once this molecule becomes part of a chevron, its hop triggers the output arm of the AND gate.

A two-input sorter, which computes both the logic AND and the logic OR of the inputs, is shown in Fig. 8. This structure contains fan-outs to duplicate the input signals for distribution to both gates and a crossover to pass the two signals through each other. The OR gate in Fig. 8 is based on a chevron that is already assembled in the initial configuration. This chevron is stabilized by two molecules blocking the normal hop of the decaying chevron. However, when either of the input cascades appends a fourth molecule to this chevron, the augmented chevron decays as shown to activate the OR gate’s output cascade. The fan-out is also based on a stabilized chevron in the initial configuration. When a fourth molecule is added to this chevron from the cascading input arm, the resulting hop produces two “overlapping” chevrons that share one CO molecule. Each of these chevrons decays and activates its respective output cascade. The crossover is more complex and uses the decay of clusters of three and four molecules not related to chevrons. One molecule in its center (Fig. 8, solid red circle) does not itself hop but transmits the information through the crossover. All of these elements are connected with linked-chevron cascades and with alignment units (labeled “A” in Fig. 8A) that provide small lateral shifts needed to connect the components. Correct operation of the crossover, fan-out, and OR gate requires orienting them with respect to the second-layer Cu atoms. We designed all of these components by developing a set of empirical rules that describe CO hop rates and directions and then using these rules to direct a trial-and-error search for the desired behavior.

The most complex cascade device we built is the three-input sorter made from 545 CO molecules (Fig. 9; see also www.research.ibm.com/resources/news/20021024_cascade.shtml). This device comprises three two-input sorters similar to the one discussed above but slightly compressed. The three outputs provide the logic AND, OR, and

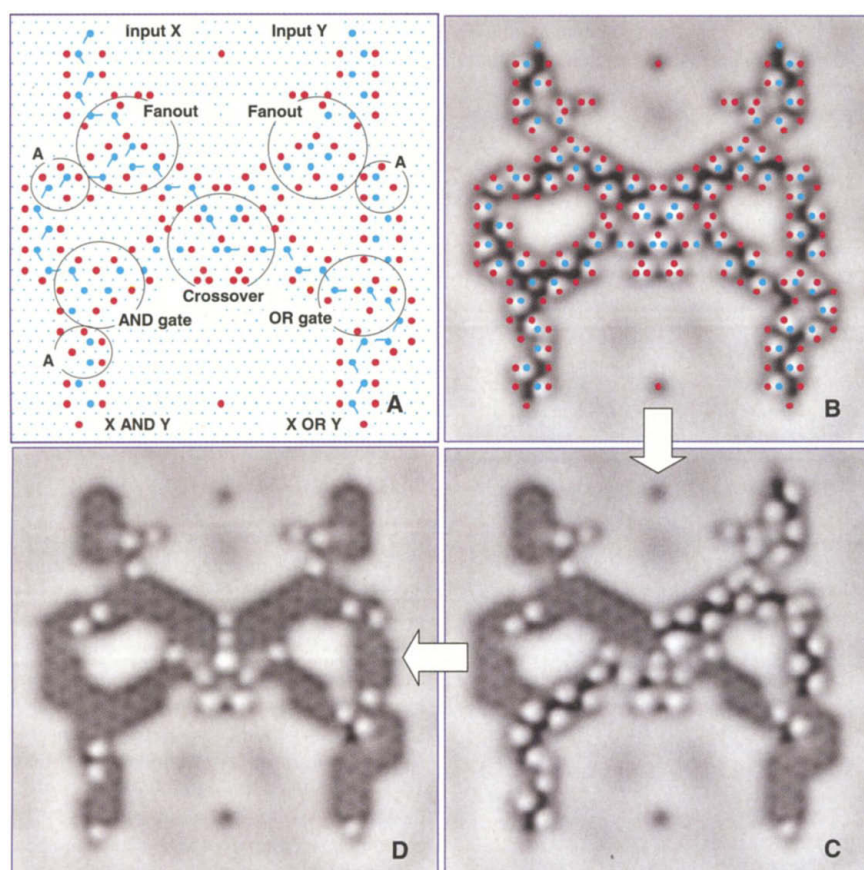


Fig. 8. Two-input sorter. (A) Model of the sorter, which computes the logic AND and logic OR of the two inputs. Color scheme is as in Fig. 7. Blue bars indicate hops that occurred when input X was triggered. The sorter consists of several components interconnected by linked-chevron cascades. (B to D) Succession of STM images (9 nm by 9 nm) ($I = 50 \text{ pA}$; $V = 10 \text{ mV}$). Starting from the initial setup (B), input X was triggered by manually moving the top CO molecule, which propagated a cascade to the OR output (C). Input Y was subsequently triggered, which propagated a cascade to the AND output, as shown in (D). The sorter also operated correctly when input Y was triggered first (not shown).

MAJORITY functions of the three inputs. We verified the operation of this structure by applying inputs in various sequences. The propagation time from input to output was ~ 1 hour at 5 K.

Conventional logic design relies on the use of a NOT gate or other inverting gate. However, implementing a NOT gate with cascades would require that all molecules in the NOT gate's output "untopple" (in analogy to dominoes) when the input cascade topples. This is not possible because the untoppled state has higher energy than the toppled state. However, it is possible to compute the NOT function with a two-input device we call a "CLOCKED-NOT" gate, in which one input, the CLOCK signal (logical 1), is known to arrive at the gate after the other input, the DATA signal. A logical 1 DATA signal functions as an interrupter of the logical 1 CLOCK signal, and a logical 0 DATA signal allows the CLOCK signal to propagate to the output unhindered; thus, the output is the logical NOT of DATA. Alternatively, the need for a NOT gate can be avoided by representing information with the dual-rail convention that is employed in some self-timed logic designs (41). In this convention, every bit of information B is represented by two cascades: One of them topples to represent $B = 0$, and the other topples to represent $B = 1$. Given inputs in this form, any logic function can be computed in a straightforward way with only AND gates and OR gates.

Cascades and computation. We now consider some features and physical properties of our implementation of cascade-based computation (and cascades in general) in the context of conventional silicon transistor-based computation. Digital signal restoration, the reestablishment of a partially degraded signal to a logical 0 or 1 before the logical content of the signal becomes ambiguous, is an essential part of digital computation that is conventionally provided by logic gates or explicit buffers (42). Digital signal restoration in our cascades is due to the bistability of the molecule's location.

We can place both upper and lower bounds on the energy dissipated per hop in CO molecule cascades. The irreversibility of our cascades implies that at least $k_B T \approx 1$ meV of energy is dissipated at each stage of the cascade. An upper limit comes from the consideration that the energy difference between two adsorption sites on a surface can, at most, be comparable to the adsorption energy, which is on the order of 100 meV. Taking 10 meV as a reasonable estimate for the energy dissipated per stage, we estimate that the three-input sorter shown in Fig. 9 would, on the average, use ~ 1 eV, or 1.6×10^{-19} J per computation. An equivalent three-input sorter implemented with next-generation (CMOS 9S) technology would, on the average, use 2×10^{-14} J per computational cycle.

At this point, it is prudent to discuss the

reliability of these devices. In the linked-chevron cascades (Fig. 2) and in the AND gates (Fig. 7), no premature hops or failures to hop as intended were observed after testing more than 5000 hops in hundreds of hours of operation. However, the more complicated structures in the fan-out, OR gate, and crossover showed occasional premature hops or unintended hops, at the rate of about one per day for the three-input sorter of Fig. 9.

Tunneling and thermally activated processes are inherently stochastic. This results in a statistical variation in the time it takes for a stochastic cascade to propagate any given number of stages. The solution to this problem is to wait until the cascade is "complete" with an acceptable probability (this being done at the cost of time). Although our CO-based molecule cascades exhibit statistical variation in propagation times, this is not necessary for cascades in general; for example, domino cascades are deterministic with predictable timing.

As implemented, our molecule cascades are exceedingly slow, especially compared to modern silicon transistor technology. In principle, the fastest possible molecule cascades could take a single vibrational period per stage, limiting their speed to $\sim 10^{-12}$ s per stage.

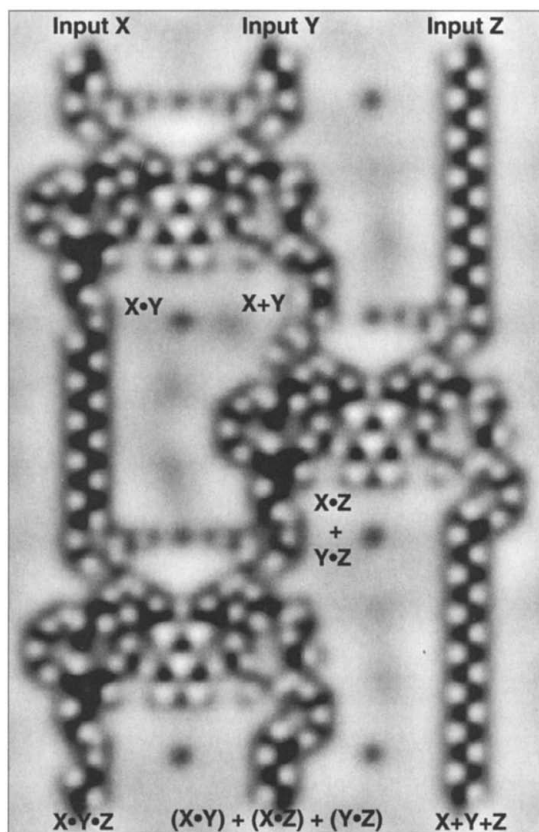
After a cascade structure is used, the molecules must be reset to their original positions before the cascade can be used again. At present, we reset the molecules one at a time with the tip of the STM. An automatic, selective reset mechanism would allow some molecules to be reset while others retain their state and act as registers, thus achieving useful data storage. Without such a reset mechanism, the utility of cascade architectures is limited to one-time applications.

A cascade need not be due to the motion of an atom or molecule; it could use any physical degree of freedom, such as charge (11, 12) or spin (13), that couples from site to site and appropriately affects the energy of the system. We anticipate that cascades using charge or spin could be reset with an electric or magnetic field, respectively. Cascades are not limited to cryogenic temperatures. Because chemical bond energies are generally large compared to room temperature, we speculate that molecular cascades can be designed to work at room temperature (43).

Any implementation of a cascade relies on design of the "energy landscape" seen by the cascading elements. Atomic and molecular cascades use chemical bonding forces to form their energy landscapes; as such, they must be atomically precise in layout of the critical elements of the cascade. This is clearly a limitation. Cascades using other physical variables and other forces need not be so precise.

The most salient feature of molecule cas-

Fig. 9. STM image (12 nm by 17 nm) of a three-input sorter in the initial setup ($I = 40$ pA; $V = 10$ mV). The symbol + denotes logic OR, and • denotes logic AND. Images with one or more inputs triggered are not shown.



acades is their size: A three-input sorter implemented in next-generation (CMOS 9S) technology requires an area of $53 \mu\text{m}^2$, whereas our cascade implementation uses only 200 nm^2 , a factor of 260,000 difference. Even if CMOS density were to continue to double every 2.5 years, it would still take 45 years to shrink to the size of these cascades.

Conclusions. Molecule cascades provide new ways to study and exploit the motion of individual molecules in nanometer-scale structures. We have shown that below 6 K, the motion of CO molecules in our cascades is due to quantum tunneling. Our results at higher temperatures suggest that thermally assisted tunneling can play an important role in chemical kinetics when Arrhenius behavior exhibits anomalously low prefactors. The extreme sensitivity of the molecule hopping rate to the height and width of the energy barrier provides opportunities for probing the interactions between an adsorbate and its surroundings. Through exactly tailored model systems, detailed comparisons with theoretical calculations should be possible. The ability to engineer the direction and rate of molecular motion has enabled us to implement extraordinarily small (albeit exceedingly slow) logic circuits.

References and Notes

- B. G. Briner, M. Doering, H.-P. Rust, A. M. Bradshaw, *Science* **278**, 257 (1997).
- R. Baer, Y. Zeiri, R. Kosloff, *Surf. Sci.* **411**, L783 (1998).
- L. J. Lauhon, W. Ho, *Phys. Rev. Lett.* **85**, 4566 (2000).
- J. Kua, L. J. Lauhon, W. Ho, W. A. Goddard III, *J. Chem. Phys.* **115**, 5620 (2001).
- J. D. Meindl, Q. Chen, J. A. Davis, *Science* **293**, 2044 (2001).
- D. Goldhaber-Gordon, M. S. Montemero, J. C. Love, G. J. Opiteck, J. C. Ellenbogen, *Proc. IEEE* **85**, 521 (1997).
- G. Y. Tseng, J. C. Ellenbogen, *Science* **294**, 1293 (2001).
- S. J. Wind, J. Appenzeller, R. Martel, V. Derycke, Ph. Avouris, *Appl. Phys. Lett.* **80**, 3817 (2002).
- Y. Huang et al., *Science* **294**, 1313 (2001).
- D. M. Eigler, C. P. Lutz, W. E. Rudge, *Nature* **352**, 600 (1991).
- C. S. Lent, P. D. Tougaw, *Proc. IEEE* **85**, 541 (1997).
- I. Amlani et al., *Science* **284**, 289 (1999).
- R. P. Cowburn, M. E. Welland, *Science* **287**, 1466 (2000).
- R. S. Braich, N. Chelyapov, C. Johnson, P. W. K. Rothmund, L. Adleman, *Science* **296**, 499 (2002); published online 14 March 2002 (10.1126/science.1069528).
- K. E. Drexler, *Nanosystems* (Wiley, New York, 1992).
- D. D. Swade, *Sci. Am.* **268**, 86 (February 1993).
- L. Bartels, G. Meyer, K.-H. Rieder, *Surf. Sci.* **432**, L621 (1999).
- Mass spectroscopic analysis of the CO isotope distribution showed an upper bound of 2% for the total amount of ^{17}O and ^{18}O .
- D. M. Eigler, E. K. Schweizer, *Nature* **344**, 524 (1990).
- M. F. Crommie, C. P. Lutz, D. M. Eigler, *Science* **262**, 218 (1993).
- G. Witte, *Surf. Sci.* **502–503**, 405 (2002).
- L. Bartels, G. Meyer, K.-H. Rieder, *Appl. Phys. Lett.* **71**, 213 (1997).
- A single CO molecule apparently decreases the local electronic density of states (LDOS) at the adsorption site at the Fermi level, which causes the feedback mechanism to move the STM tip closer to the surface in order to keep a constant tunnel current. In contrast, the dimer shows an increase in the LDOS between the two CO molecules.
- The hopping rates were influenced by the presence of the tip (either slowed or sped up, depending on the tip position) even at low tunnel current ($I \approx 50 \text{ pA}$) and bias voltage between $V = 5 \text{ mV}$ and $V = 50 \text{ mV}$. The size of the influence depends primarily on the tip height (rather than on I or V) when V is kept well below the 35-meV vibrational excitation.
- N. Knorr et al., *Phys. Rev. B* **65**, 115420 (2002).
- B. C. Stipe, M. A. Rezaei, W. Ho, *Science* **280**, 1732 (1998).
- J. I. Pascual et al., *Surf. Sci.* **502–503**, 1 (2002).
- L. J. Lauhon, W. Ho, *Phys. Rev. B* **60**, R8525 (1999).
- R. Raval et al., *Surf. Sci.* **203**, 353 (1988).
- J. Braun et al., *J. Chem. Phys.* **105**, 3258 (1996).
- The step in conductance is $\sim 20\%$ at $|V| = 35 \text{ mV}$ and $\sim 15\%$ at $|V| = 4 \text{ mV}$ for CO arranged in the $\sqrt{3}$ by $\sqrt{3}$ lattice, but only half as large for isolated CO molecules. We did not observe the 41-mV CO to Cu external stretch mode.
- The exponent in the WKB approximation for the tunneling rate can be evaluated for one isotope by using the measured rate and assuming an attempt rate for tunneling on the order of the external vibrational frequencies ($A_{\text{OT}} = 5 \times 10^{12} \text{ s}^{-1}$). The tunneling mass ratio is then determined with the rate for the other isotope.
- Tunneling and classical over-the-barrier processes both depend on the stiffness of the full many-dimensional potential energy surface in the coordinates perpendicular to the reaction path. This makes it difficult to determine the value, and even the sign, of isotope shifts; for example, modes that are stiffer in the barrier than in the initial state favor passage of heavier isotopes.
- R. Baer, Y. Zeiri, R. Kosloff, *Phys. Rev. B* **54**, R5287 (1996).
- S. Ovesson et al., *Phys. Rev. B* **64**, 125423 (2001).
- J. V. Barth, H. Brune, B. Fischer, J. Weckesser, K. Kern, *Phys. Rev. Lett.* **84**, 1732 (2000).
- J. V. Barth, *Surf. Sci. Rep.* **40**, 75 (2000).
- G. X. Cao, E. Nabighian, X. D. Zhu, *Phys. Rev. Lett.* **79**, 3696 (1997).
- P. J. Price, *Am. J. Phys.* **66**, 1119 (1998).
- F. Wittl et al., *J. Chem. Phys.* **98**, 9554 (1993).
- C. L. Seitz, in *Introduction to VLSI Systems*, C. A. Mead, L. A. Conway, Eds. (Addison-Wesley, Reading, MA, 1980), p. 218–262.
- R. Landauer, *Physica A* **168**, 75 (1990).
- Chain polymerization initiated with an STM tip has been demonstrated at room temperature (44).
- Y. Okawa, M. Aono, *J. Chem. Phys.* **115**, 2317 (2001).
- We thank J. P. Sethna for useful discussions and preliminary analysis of these results and G. Northrop for his design of a three-input sorter implemented in CMOS 9S technology.

30 July 2002; accepted 4 October 2002

Published online 24 October 2002;

10.1126/science.1076768

Include this information when citing this paper.

Structural Basis for the Transition from Initiation to Elongation Transcription in T7 RNA Polymerase

Y. Whitney Yin¹ and Thomas A. Steitz^{1,2,3*}

To make messenger RNA transcripts, bacteriophage T7 RNA polymerase (T7 RNAP) undergoes a transition from an initiation phase, which only makes short RNA fragments, to a stable elongation phase. We have determined at 2.1 angstrom resolution the crystal structure of a T7 RNAP elongation complex with 30 base pairs of duplex DNA containing a "transcription bubble" interacting with a 17-nucleotide RNA transcript. The transition from an initiation to an elongation complex is accompanied by a major refolding of the amino-terminal 300 residues. This results in loss of the promoter binding site, facilitating promoter clearance, and creates a tunnel that surrounds the RNA transcript after it peels off a seven-base pair heteroduplex. Formation of the exit tunnel explains the enhanced processivity of the elongation complex. Downstream duplex DNA binds to the fingers domain, and its orientation relative to upstream DNA in the initiation complex implies an unwinding that could facilitate formation of the open promoter complex.

Despite structural differences, the 99-kD single-subunit RNA polymerase from the bacteriophage T7 (T7 RNAP) and the multisubunit cellular RNAPs share numerous functional characteristics. Both families of RNAPs have initiation and elongation phases of transcription (1, 2). During the initiation phase, RNAP binds to a specific DNA promoter, opens the duplex

at the transcription start site, and initiates RNA synthesis de novo. Transcription during this phase is unstable and characterized by repeated abortive initiation events that produce short RNA fragments [2 to 6 nucleotides (nt)] (3, 4). After synthesis of 10- to 12-nt-long RNA, the polymerase enters the elongation phase and completes transcription of the mRNA processively without dissociating until termination. There are significant biochemical differences between the initiation and elongation states. Footprinting assays show differences in DNA protection (5–7). The T7 RNAP-DNA complex is substantially more stable in the elongation phase (4, 8, 9),

¹Department of Molecular Biophysics and Biochemistry, ²Department of Chemistry, ³Howard Hughes Medical Institute, Yale University, 266 Whitney Avenue, New Haven, CT 06520–8114, USA.

*To whom correspondence should be addressed. E-mail: eatherton@csb.yale.edu